On the effect of asymmetrical trait inheritance on models of trait evolution

Pablo Duchen[1], Michael L. Alfaro[2], Jonathan Rolland[1,3], Nicolas Salamin[1,*], Daniele Silvestro[1,4,5,*]

1. Department of Computational Biology, University of Lausanne, Quartier Sorge, 1015 Lausanne, Switzerland.

2. University of California Los Angeles (UCLA). College Life Sciences - Ecology and Evolutionary Biology. Los Angeles, United States.

3. Department of Zoology, University of British Columbia, #4200-6270 University Blvd, Vancouver, BC, Canada.

4. Department of Biological and Environmental Sciences, University of Gothenburg, Carl Skottsbergs gata 22B, Gothenburg 41319, Sweden.

5. Gothenburg Global Biodiversity Centre, Box 461, SE-405 30 Gothenburg, Sweden.

[*] co-last authors.

Correspondence:

Name: Pablo Duchen

email: pablo.duchenbocangel@unil.ch

Running head: Trait inheritance in models of macroevolution

Abstract

Current phylogenetic comparative methods modeling quantitative trait evolution generally assume that, during speciation, phenotypes are inherited identically between the two daughter species. This, however, neglects the fact that species consist of a set of individuals, each bearing its own trait value. Indeed, because descendent populations after speciation are samples of a parent population, we can expect their mean phenotypes to randomly differ from one another potentially generating a "jump" of mean phenotypes due to asymmetrical trait inheritance at cladogenesis. Here, we aim to clarify the effect of asymmetrical trait inheritance at speciation on macroevolutionary analyses, focusing on model testing and parameter estimation using some of the most common models of quantitative trait evolution. We developed an individual-based simulation framework in which the evolution of species phenotypes is determined by trait changes at the individual level accumulating across generations and cladogenesis occurs then by separation of subsets of the individuals into new lineages. Through simulations, we assess the magnitude of phenotypic jumps at cladogenesis under different modes of trait inheritance at speciation. We show that even small jumps can strongly alter both the results of model selection and parameter estimations, potentially affecting the biological interpretation of the estimated mode of evolution of a trait. Our results call for caution interpreting analyses of trait evolution, while highlighting the importance of testing a wide range of alternative models. In the light of our findings, we propose that future methodological advances in comparative methods should more explicitly model the intra-specific variability around species mean phenotypes and how it is inherited at speciation.

Introduction

Understanding the mechanisms underlying the evolution of phenotypic traits is fundamental when addressing questions about functional diversity, ecological interactions, and the overall build-up of biodiversity (Futuyma and Agrawal, 2009; Katzourakis et al., 2009; Campbell and Kessler, 2013). Inferences about the processes governing phenotypic changes are facilitated by the use of macroevolutionary models, which deal with the evolution of phenotypic traits among related species (Stanley, 1979; Lande, 1980; Felsenstein, 1985, 2004). These macroevolutionary models are able to infer the evolution of a phenotype under a variety of scenarios including neutral or adaptive evolution (Lande, 1976; Beaulieu et al., 2012), as well as early and rapid phenotypic differentiation (Harmon et al., 2010; O'Meara, 2012). These models have been used to address a variety of evolutionary processes, helping us understand, for instance, body size evolution in mammals (Venditti et al., 2011; Slater, 2013), adaptation in *Anolis* lizards (Losos, 2011), evolutionary processes in extinct and extant vertebrates (Wagner, 2017; Silvestro et al., 2018), or changes in flower morphology and pollination syndromes (Wasserthal, 1997; Futuyma and Agrawal, 2009; Serrano-Serrano et al., 2017).

The simplest macroevolutionary model of trait evolution assumes that a trait X evolves following a random walk process, which is typically modeled by Brownian Motion (BM; Felsenstein, 1973). Under BM, the expected change in trait X is normally distributed and depends on time t and a rate parameter σ^2, such that $dX_t \sim \mathcal{N}(0, \sigma^2 t)$, where the variance $\sigma^2 t$ increases monotonically with time. We can also assume that traits evolve toward an optimal value and that phenotypic variance is constrained around that optimum, which leads to a process that is typically modeled by the Ornstein-Uhlenbeck (OU) model (Hansen, 1997). Many extensions of the BM and OU models have been developed and these include rate changes across clades (Eastman et al., 2011) or through time (Harmon et al., 2010), evolutionary

51   trends (Slater et al., 2012; Silvestro et al., 2018), and trait boundaries (Boucher and

52   Démery, 2016). Other extensions of BM are designed to identify bursts or "jumps" in

53   the rate of evolution using Lévy processes. These approaches couple BM evolution

54   with Poisson jumps (Landis et al., 2012; Duchen et al., 2017) to account for the

55   presence of large changes in the rate of evolution that could capture shifts to new

56   adaptive zones related to the dispersal into new geographic areas (as described by

57   Simpson, 1944), key innovations, or by rapid climatic changes (Simpson, 1944;

58   Hansen and Martins, 1996). The BM and OU models, and their extensions, all

59   describe the anagenetic change of a trait as a continuous-time Markov chain along

60   each branch of the tree, while the descendent nodes following a branching event

61   inherit the last phenotypic value of the parent species (Felsenstein, 1973). In other

62   words, at speciation, most current models of trait evolution assume that the

63   descendent species inherit identically the phenotype of their last common ancestor

64   (Felsenstein, 1973; O'Meara et al., 2006) leading to a symmetrical trait inheritance

65   between the daughter lineages.

66   Macroevolutionary models use species as the units of evolution and aim to model

67   the evolution of the mean phenotype of each species. This emphasis on a single trait

68   value, which makes the commonly used models of trait evolution highly tractable,

69   masks the fact that species are composed by sets of individuals possessing

70   non-identical trait values.

71   Because daughter populations after speciation are samples of a parent population

72   ((Fig. 1A)), we can expect their mean phenotypes to differ from one another and

73   from the parent mean due to random demographic events and/or differential

74   segregation of the trait values within the incipient species (Uyeda et al., 2011;

75   Kostikova et al., 2016). If the two mean phenotypes of the descendants differ from

76   the parent phenotype, the difference will generate "jumps" of the mean phenotype at

77   cladogenesis and lead to asymmetrical trait inheritance. Strong asymmetrical trait

78   inheritance is expected when the trait is itself involved or even driving the speciation

3

79 process (Fig. 1D), such as floral size and pollination syndromes in flowering plants

80 (Wasserthal, 1997; Serrano-Serrano et al., 2015), morphology in insect genitalia

81 (Schilthuizen, 2003; Ayoub et al., 2005), or color patterns in cyclids (Galis and Metz,

82 1998) and *Heliconius* butterflies (Jiggins et al., 2008). Even if the trait is not directly

83 involved in the speciation process, geographic gradients of phenotypes and allopatric

84 or peripatric speciation events could generate cladogenetic jumps in the mean

85 phenotypes (Fig. 1B,C). For example, current subspecies of brown bear display

86 substantial differences in their body mass (e.g. Kingsley et al., 1983; McCarthy et al.,

87 2009). If they were to become independent species, the mean body size of each of the

88 new species would differ from each other, and more importantly, would not be equal

89 to the mean body mass of all brown bears. Therefore the assumption of identical

90 inheritance in this case would be a poor description of the speciation process.

91 Models accounting for phenotypic jumps at speciation have been proposed. For

92 instance, Pagel (1999) used a transformation of the elements of the phylogenetic

93 variance-covariance matrix, called κ, to model cladogenetic jumps in the trait value

94 by transforming the branch lengths of a phylogeny to modulate the importance of

95 cladogenetic events versus anagenetic evolution. An alternative model introduced a

96 Bayesian approach to estimate rates of both anagenetic and cladogenetic phenotypic

97 evolution (Bokma, 2008). However, the empirical application of these models is

98 limited and it remains unclear whether the models can capture the signal of

99 asymmetrical trait inheritance at speciation.

100 Here, we aim to clarify the effect of different modes of asymmetrical trait

101 inheritance at speciation on macroevolutionary analyses. We focus in particular on

102 the fit of the models and the estimation of the specific parameters using four models

103 of phenotypic evolution: BM, OU, Lévy, and κ. To accomplish this, we first

104 developed an individual-based simulation framework in which the evolution of species

105 phenotypes is determined by trait changes at the level of individuals accumulating

106 across generations. Cladogenesis occurs by separation of two subsets of the

4

107   individuals into new lineages. The inherited phenotypes of the descendent species is

108   thus the mean of the individuals' trait values and might differ from one another and

109   from the parent phenotype. Using simulations, we assess the magnitude of expected

110   phenotypic jumps at cladogenesis under different modes of trait inheritance at

111   speciation. We show that these jumps can strongly alter both model selection and

112   parameter estimations in all the widely used macroevolutionary models of trait

113   evolution.

Materials and Methods

114

115   To show the effect of asymmetrical trait inheritance on model fit and parameter

116   estimation, we developed an individual-based forward simulator. This allows us to

117   model the evolution of mean species phenotypes through the microevolutionary

118   change across individuals within species and their segregation at speciation. We

119   simulated trait values forward in time under two types of fitness landscapes: flat

120   (where all individuals have the same fitness regardless of their trait value) and normal

121   (where individuals with trait values closer to the optimum peak have higher fitness

122   than other individuals). We applied for each type of landscape different modes of

123   speciation, which determine the partitioning of individuals from a parent species into

124   two descendent species. The forward simulations generate changes at the generational

125   time scale (the phenotypes of the individuals within each species) that translate into

126   macroevolutionary processes when looking at the mean phenotype of species and

127   their phylogenetic relationships resulting from the speciation process. Our

128   simulations thus provide a framework linking micro with macroevolutionary processes

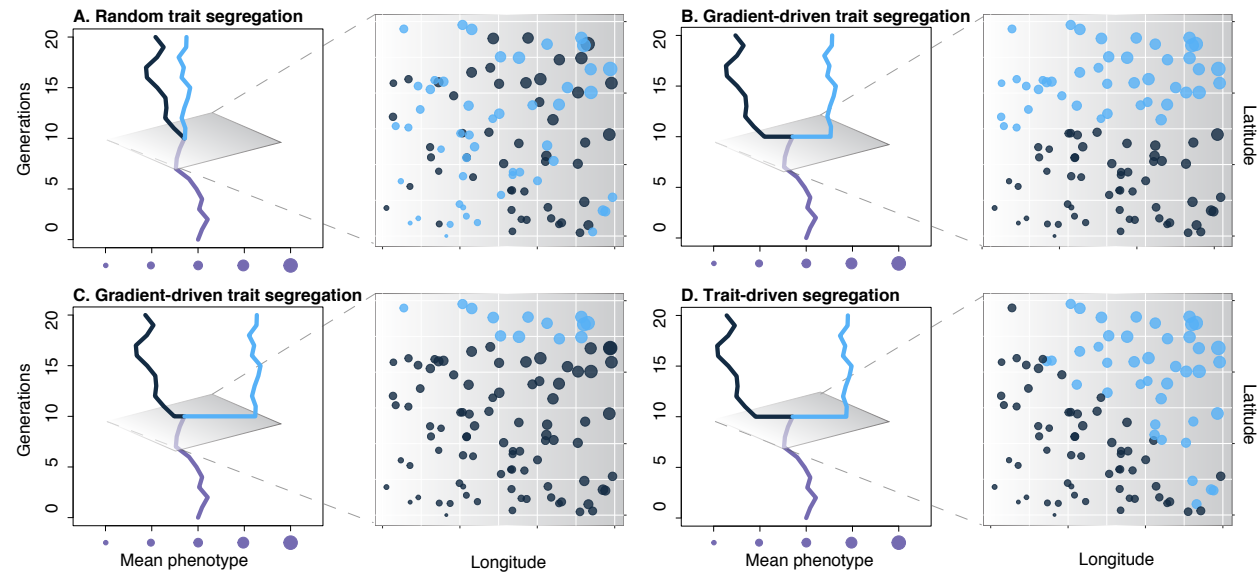129   for a quantitative trait.

Figure 1: **Four different scenarios of trait inheritance at speciation.** Left panels: Evolutionary history of the mean phenotype before and after a speciation event. Right panels: Geographical distribution of individuals at the speciation event depicted in the left panel. Bubbles represent the spatial distribution of individuals splitting from a parent population into two species (gray and light blue). The size of the bubbles is proportional to each individual's phenotype. In this example, individual phenotypes follow a geographical gradient with smaller trait values on the lower-left part of the geographic range and larger trait values on the upper-right part. Under random segregation (A) speciation is not driven by the trait displayed here nor by geography and might result from a change in an uncorrelated trait, e.g. flowering time. The mean phenotypes of the two descendants are expected to be equal with some stochasticity. Speciation occurring by geographic isolation, e.g. allopatric (B) or peripatric (C) may result in asymmetrical trait inheritance even though the trait itself is not the cause of speciation. Finally, if the trait is itself driving the speciation we can expect a full segregation of phenotypes at speciation (D). In the present study, we analysed cases A and D, which represent the extremes in terms of the size of cladogenetic jumps.

Modes of trait inheritance at speciation

We considered two modes of trait inheritance at speciation: "Random Segregation at Speciation" (RSS) and "Trait-driven Segregation at Speciation" (TSS). Under the RSS scenario, at each speciation event, the individuals of the parent population are randomly assigned to each daughter lineage (Fig. 1A). This corresponds to cases in which the phenotype represented by the trait of interest is completely independent of speciation. Conversely, under the TSS scenario, individuals of a parent population are split into two daughter lineages based on their phenotype and an arbitrary threshold defined a priori (Fig. 1D). The RSS and TSS constitute the extreme

6

139 scenarios of how traits can be segregated during the split of a parent lineage and will

140 generate the smallest and largest jumps, respectively. Cladogenetic jumps of

141 intermediate size can also result from spatial gradients of phenotypic traits, captured

142 by allopatric or peripatric speciation (Fig. 1B and C).

Death probabilities

144 Before the full description of the forward simulations (modes of reproduction,

145 generational changes, etc.) and to unburden the explanation of the simulation

146 algorithm, we will detail here the factors influencing the death probabilities of the

147 simulated individuals.

148 The death probability of each individual (δ) is determined by the combined effect

149 of three factors: fitness, distance from the species-specific mean phenotype, and

150 species-specific carrying capacity. Each of these factors contributes to the death

151 probability of an individual by a specific quantity, such that

$$\delta = \min(d_f + d_s + d_k, 1), \tag{1}$$

152 where d_f, d_s, and d_k are the death probabilities by fitness, distance from the

153 species-specific mean phenotype, and carrying capacity, respectively (see below).

Death probability determined by fitness We used a fitness landscape to

155 describe the fitness of individuals as a function of their phenotypic trait value

156 (Simpson, 1944; Arnold et al., 2001; Svensson and Calsbeek, 2012; Boucher et al.,

157 2017). The shape of the fitness landscape defines the survival probability of an

158 individual and, as explained at the beginning of the Methods, we used two types of

159 landscapes. First, we assumed that fitness was independent of the trait value, which

160 corresponds to a flat landscape. Because the trait does not affect fitness under a flat

161 landscape, its evolution is expected to follow a neutral process as captured by the BM

7

162   model (Felsenstein, 1988). Second, we assumed a normally-shaped fitness landscape,

163   where there is an optimal phenotype (the peak of the landscape) for which the fitness

164   is highest. This landscape can represent the distribution of fitness under stabilizing

165   selection (Beaulieu et al., 2012; O'Meara and Beaulieu, 2014), which is one of the

166   biological processes resulting in an OU mode of evolution (Lande, 1976; Felsenstein,

167   1988; Hansen and Martins, 1996; Hansen, 1997).

168   In our simulations, the fitness landscape affects the death probability of each

169   individual by an amount d_f. Under a flat landscape, the death probability is

170   independent of the trait value and set to a constant $d_f = c$ (Table 1). Under a

171   normally-distributed landscape, the death probability of an individual depends on the

172   position of the phenotypic trait value on the fitness landscape, which is described by

173   an optimum θ and a variance σ_f^2. Thus, the fitness-based death probability of an

174   individual with phenotype x is

$$d_f = 1 - \left(\frac{f(x|\theta, \sigma_f^2)}{f(\theta|\theta, \sigma_f^2)} (1-c) \right), \tag{2}$$

175   where $f(x|\theta, \sigma_f^2)$ is the probability density function of a normal distribution with

176   mean θ, and variance σ_f^2 (a complete list of the parameters used in this study is given

177   in Table 1). Under this formulation, the death probability of an individual with

178   optimal phenotype (i.e. $x_1 = \theta$) is equal to c.

179   **Death probability determined by the distance to the species mean**

180   We added a constraint to limit the intra-specific variance under the assumption that,

181   regardless of the fitness landscape, there is selection against outliers diverging from

182   the species' mean (Harvey et al., 1991; Garland et al., 1993; Futuyma, 2010). To

183   achieve this, we set the death probability d_s of an individual with phenotype x to a

184   function of its species mean phenotype at time t $(m(t))$ and of a fixed intra-specific

variance σ_s^2. Thus, this death probability is

$$d_s = 1 - \left(\frac{f(x|m(t), \sigma_s^2)}{f(m(t)|m(t), \sigma_s^2)} (1 - c) \right), \tag{3}$$

where $f(x|m(t), \sigma_s^2))$ is the probability density function of a normal distribution with mean $m(t)$, and variance σ_s^2 (Table 1). While the intra-specific variance is assumed to be constant over time, the species mean, $m(t)$, is not subject to any constraints but simply computed as the empirical mean of the phenotypes of the individuals.

Death determined by the carrying capacity Finally, the population growth within a species is controlled by a species-specific carrying capacity K (Etienne et al., 2011). This is achieved by changing the death probability d_k of all individuals within a species based on their current population size n and its proximity to K, such that

$$d_k = (g - 1)\frac{n}{K}, \tag{4}$$

where g is the growth rate of that species.

Forward simulations

For all combinations of fitness landscapes and modes of trait inheritance (RSS-flat, RSS-normal, TSS-flat, and TSS-normal), we ran an individual-based forward simulator of continuous traits which works as follows:

1. **Initialization.** At generation $i = 1$, we have a starting population of $n = 200$ individuals assigned to Species 1, with trait values drawn from a normal distribution with mean μ and standard deviation σ_0 (Table 1).

2. **Change from one generation to another.** Individuals of generation $i = 1$ are replaced by a number of offspring based on a Poisson distribution with rate g, such that $n_{i+1} \sim n_i \times Pois(g)$. The trait values assigned to each individual of

9

Table 1: Parameter definitions. The arbitrary values used in our simulations are given for the parameters used in the forward simulations. Model parameters that are estimated from macroevolutionary models do not have any input value and are thus shown with a "-" sign.

Parameter	Definition	Default value
μ	Root state	0
σ_G^2	Parent-offspring variance	0.01
c	Per individual baseline death probability (Eqs. (3),(2))	0.00001
σ_0	Initial standard deviation	0.01
g	Growth rate	1.2
λ_s	Speciation rate per lineage	0.0001
σ_f^2	Variance of the normal fitness landscape	25
σ_s^2	Intraspecific variance	1
θ	Trait optimum	5
θ_{OU}	Trait optimum under OU	-
κ	Statistic of the κ model	-
α	Rate of mean reversion (or selective strength)	-
σ_{BM}^2	Rate of evolution under BM	-
σ_{OU}^2	Rate of evolution under OU	-
σ_{LE}^2	Rate of evolution under Lévy	-
λ	Jump rate	-

205   the new generation will be normally distributed with mean set to the value of

206   the parent individual and variance σ_G^2. Individuals of the new generation die

207   with probability δ (Eq. (1)). Based on this birth-death equilibrium, the overall

208   population might go extinct or grow until a carrying capacity K is reached (see

209   section *Death determined by the carrying capacity*). We defined K to be large

210   enough to obtain a stable mean phenotype for each lineage. The variance of the

211   normal landscape σ_f^2 was set to 10,000 to ensure that the initial population will

212   not start at a too-low fitness position (Table 1). This landscape yields a 1.25%

213   increase in death rate for a phenotype $= 0$ (the predefined root state) compared

214   to the death rate at phenotype $= 5$ (the predefined trait optimum).

215   3. **Speciation.** Speciation occurs with probability λ_s per generation per lineage.

216   At speciation, a given number of individuals from the parent species are

217   assigned a new species label. The initial number of individuals for the new

218   species is drawn from $\mathcal{U}(100, n - 100)$, where n is the population size of the

219   parent species. We note that speciation leads to a temporary reduction in

220   population size in the two daughter lineages, but with the growth rate set to 1.2

221   (Table 1), we ensure that the populations grow back rapidly until the carrying

222   capacity is reached again within a few generations (Fig. SI-9). The way

223   individuals are chosen to become a new species is described in the previous

224   section *Modes of trait inheritance at speciation*.

225   4. We repeat steps 2 and 3 for every species for a total of 100,000 generations or

226   until 100 species are generated. We then output the following files and

227   statistics: species phylogenetic tree in newick format, mean (and variance) trait

228   values per species at the tips of the phylogeny, mean (and variance) trait values

229   per species at intermediate generations along the tree, full trait values along the

230   entire phylogeny (optional setting), population sizes per species, and mean (and

231   variance) phenotypic-trajectory plots.

232   For each scenario (RSS-flat, RSS-normal, TSS-flat, and TSS-normal), we

233   simulated 100 data sets, from which we extracted the species level phylogenies and

234   trait values for further analyses. We summarized the sizes of jumps generated under

235   the different simulation scenarios by computing the absolute difference between the

236   phenotypes of the two daughter lineages following each speciation event.

Fitting macroevolutionary models

238   To quantify the effect of the different simulation settings on species-level analyses

239   of trait evolution, we analyzed the simulated phylogenetic trees and phenotypic

240   values using the function *fitContinuous* from the R library *geiger* (Pennell et al.,

241   2014) under different macroevolutionary models in a maximum likelihood framework.

242   We fit the models BM, OU, κ (indicated as KA in the figures), and we added also a

243   white noise (WN) model, which indicates the absence of phylogenetic signal in the

11

244 trait values. From all these models we calculated their respective AICc's and

245 parameter estimates (Table 1). Additionally, we analyzed the simulated data under a

246 Lévy (LE) jump model using the software *levolution* (Duchen et al., 2017) and

247 obtained the respective AICc and model parameters σ_{LE} and jump rate λ. Since

248 there is no implementation of the Bayesian/MCMC model by Bokma (2008), we did

249 not include it in the current analysis. However, given that our simulations comprise

250 complete phylogenies and complete trait data, it is expected that the κ model will

251 capture this signal equally well (Harmon, 2018).

252 We then assessed the effect of the different speciation scenarios on the estimation

253 accuracy of the following macroevolutionary parameters: the rate of evolution under

254 BM σ_{BM}^2, OU σ_{OU}^2, and Lévy σ_{LE}^2, the jump rate λ, the κ parameter, the selective

255 strength α, and the optimum trait value θ_{OU}. To quantify the accuracy of the

256 estimated σ_{BM}^2 and σ_{LE}^2 we ran the simulator again for 10,000 generations and

257 calculated the true evolutionary rate σ_{true}^2 as the average change in the trait value per

258 generation along a lineage. We then computed the relative error of the estimates as

259 $(\sigma_{BM}^2 - \sigma_{\text{true}}^2)/\sigma_{\text{true}}^2$. To quantify the accuracy for the estimated selective strength α

260 we compared it to the true selective strength α_{true} using the estimator of Duchen

261 et al. (2018), which takes as input the vector of mean phenotypes over time for each

262 species. Finally we computed the accuracy of the optimum trait value as $(\theta_{OU} - \theta)/\theta$.

Results

264 We studied the effect of asymmetrical trait inheritance on the fit of

265 macroevolutionary models of phenotypic evolution. Our individual-based simulations

266 generated species trees reflecting a pure-birth process, as shown by the

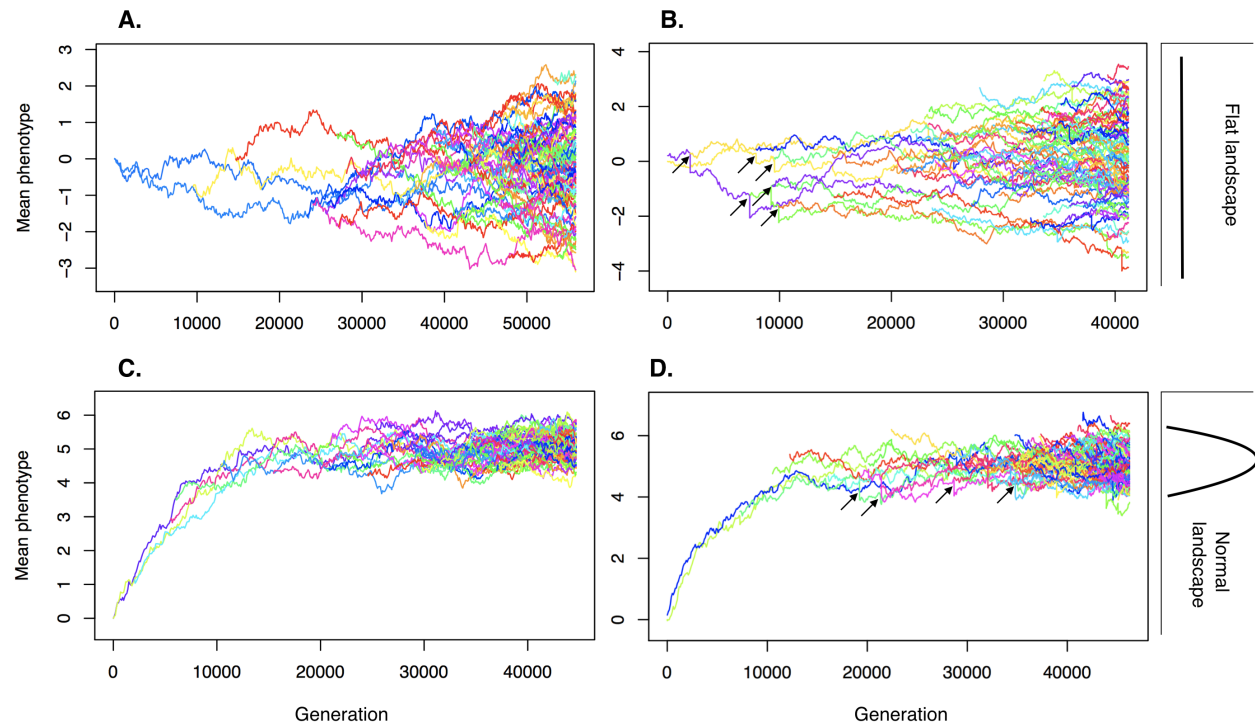267 lineage-through-time (LTT) plots generated for all scenarios (Fig. SI-7).

12

Figure 2: Examples of phenotypic trajectories under all four scenarios: A) RSS-flat, B) TSS-flat, C) RSS-normal, and D) TSS-normal. Different colors represent different species. Some examples of cladogenetic jumps (for scenarios B and D) are pointed with black arrows. The bulk of the jumps are covered by all lineages, but a quantification of their sizes is shown in Fig. 3.

Phenotypic trajectories   The simulated phenotypic trajectories show differences between different scenarios. The first clear distinction lies between flat and normal landscapes. Flat landscapes produce neutrally evolving traits without trends and generate BM-like phenotypic trajectories (Fig. 2A, B). In contrast, with normal landscapes species mean phenotypes evolve toward the value with maximum fitness (Fig. 2C, D), generating an OU-like process (Revell, 2012).

When individuals were assigned to new species independently of the trait value (RSS scenarios), the trait inheritance at speciation is nearly symmetrical, as shown by the lack of noticeable jumps in the phenotypic trajectories (Fig. 2A, C). Conversely, if individuals were assigned to new species based on a threshold in the trait value (TSS scenarios), the trait inheritance at speciation is asymmetrical and results in visible jumps in species phenotypes (Fig. 2B, D). The jump sizes between

13

²⁸⁰ the daughter species under our simulation settings were on average 30 times higher in

²⁸¹ the TSS scenarios compared to the RSS scenarios (Fig. 3).
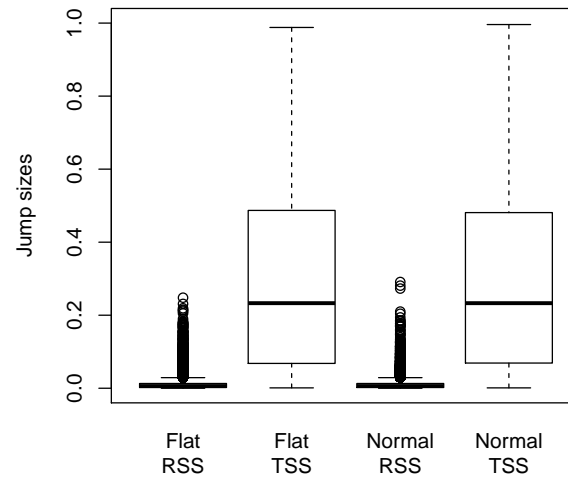

Figure 3: Absolute jump sizes for every scenario. Boxplots represent the distribution of jump sizes for all speciation events across all simulations for a given scenario. Here, the size of a jump is simply the absolute difference between the starting values of the two daughter lineages.

²⁸² **Effect of RSS and TSS on model fit**   To analyze the effect of the different

²⁸³ modes of trait segregation at speciation and fitness landscapes on model fit, we fitted

²⁸⁴ BM, OU, Lévy, κ and WN models to the simulated trees and tip trait data. Under

²⁸⁵ the flat RSS scenario, BM was the most frequently selected model (68.6%), followed

²⁸⁶ by κ (13.7%), OU (10.8%), and Lévy (6.9%; Fig. 4). Under the flat TSS scenario, κ

²⁸⁷ was the preferred model in 97.0% of the simulations, followed by Lévy (3.0%). The

²⁸⁸ normal RSS scenario shows over 98% of OU as a preferred model and almost no cases

²⁸⁹ of the other models. Finally, for the normal TSS scenario, the WN model was

²⁹⁰ preferred in 54.5% of the cases, OU being preferred 34.5% of the time, κ 6.2%, and
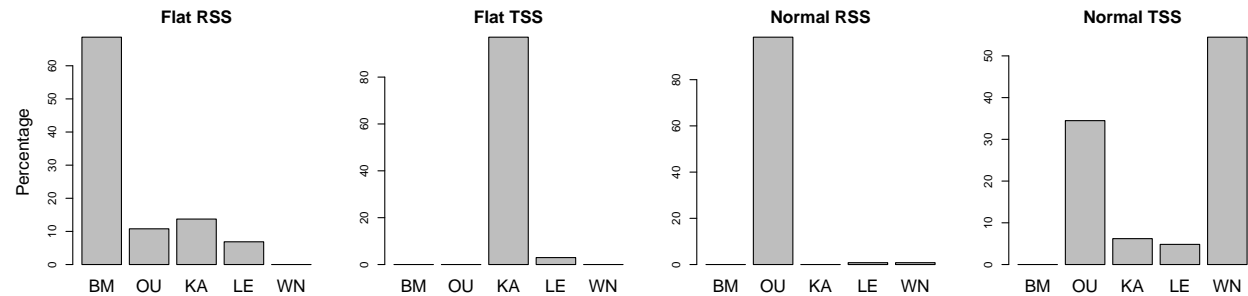
²⁹¹ Lévy 4.8% (Fig. 4).

14

Figure 4: Model fit under all four scenarios. Bars represent the percentage of simulations that were best fit by a given model. Abbreviations: BM = Brownian Motion, OU = Ornstein-Uhlenbeck, KA = Kappa, LE = Lévy, WN = White Noise. The second best fit is given in Fig. SI-8.

Effect of RSS and TSS on parameter estimation   Analyses of data sets

simulated under a flat RSS scenario resulted in a slight overestimation of the

evolutionary rates under both the BM and Lévy models (Table 2). The

overestimation was 50% lower under the Lévy model (Fig. 5A). This indicates that

the Lévy model was able to identify, at least to some extent, the jumps generated

under asymmetrical segregation at speciation. Simulations obtained from the flat

TSS scenario resulted in a 2.5-fold overestimation of the evolutionary rate under BM

and a 1.7-fold overestimation under Lévy (Table 2).

In simulations with a normal landscape, the trait optimum was accurately

recovered under all scenarios (Fig. 5A; Table 2), that is regardless of the segregation

scenario at speciation. The strength of selection of the OU process was only slightly

underestimated under the RSS scenario, while it was strongly overestimated (16-fold)

under the TSS scenario (Fig. 5F; Table 2).

Although for other parameters we could not compute accuracy (as the true values

could not be derived analytically or empirically from the simulations), the estimated

values differed vastly between speciation modes (Fig. 5), indicating that segregation

at speciation has a large effect on the macroevolutionary modeling of trait evolution.

For instance, the κ parameter was lower in TSS when compared to RSS (Fig. 5C),

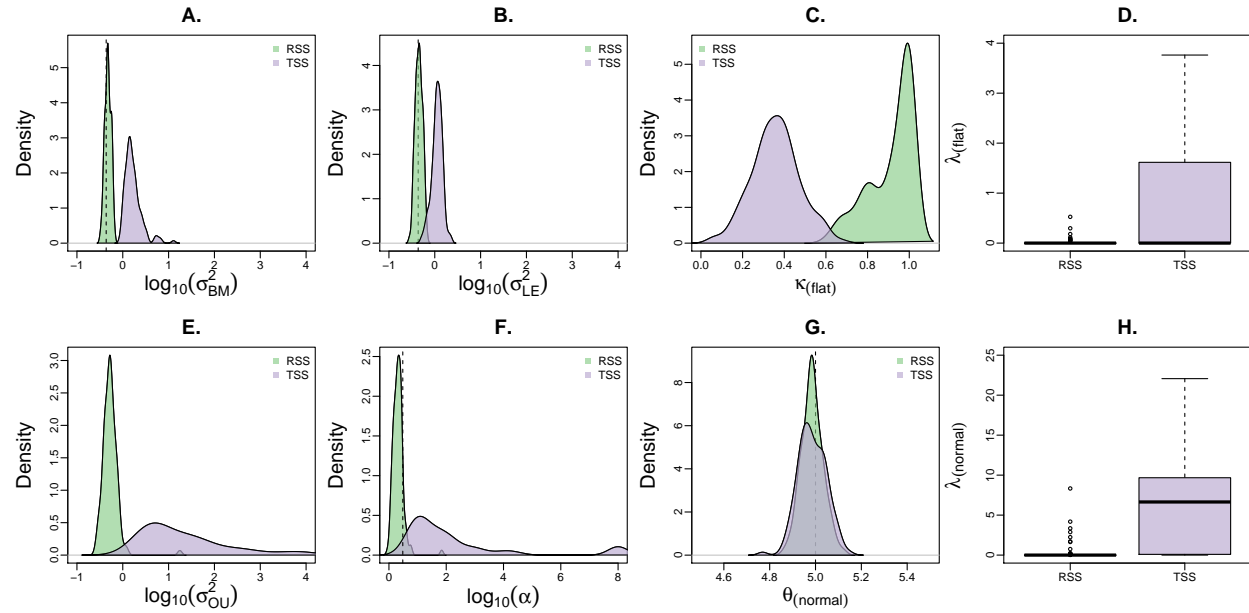which is expected since κ values tend to zero when most of the variation is

Figure 5: Parameter estimates of *fitContinuous* of various model parameters. Green (purple) distributions represent the estimates of all TSS (RSS) simulations. Abbreviations: σ^2=evolutionary rate, κ=parameter kappa, α=selective strength, λ=jump rate, and θ=optimum. Mean relative error (MRE) between RSS or TSS and the true value, or mean magnitude difference (MMD) between RSS and TSS distributions are depicted in Table 2.

accumulated at speciation events (Pagel, 1999). Finally, the jump rate of the Lévy model (λ) was much higher in TSS than in RSS simulations, as expected given the increased amount of phenotypic jumps at speciation.

Discussion

We explored the effects of asymmetrical trait inheritance on macroevolutionary analyses using phylogenetic comparative methods. We model the asymmetry of trait inheritance at speciation as a result of the segregation of individuals from a parent population into two daughter lineages. We showed that even small phenotypic jumps at cladogenesis can have profound effects on both model testing and parameter estimation using widely-used macroevolutionary models, most of which implicitly assume identical trait inheritance at speciation (Felsenstein, 1988; Hansen and

16

Table 2: Median relative error (MRE) of some parameter estimates.

Parameter	MRE (RSS)	MRE (TSS)
σ^2_{BM}	0.09	2.50
σ^2_{LE}	0.04	1.66
θ_{OU}	-0.004	-0.005
α	-0.33	16.11

Martins, 1996).

A simulation framework   We built a simulation framework that captures some of the main evolutionary processes that affect the micro- and macroevolutionary history of a quantitative trait. By tracking the phenotype of each individual for thousands of generations and across all the branches of a phylogenetic tree, we studied the effect of asymmetrical trait inheritance at speciation on model fit and parameter estimation of traditional macroevolutionary models. The current version of our simulator is set to work with haploid taxa, two fitness landscapes: flat and normal, and two modes of trait inheritance at speciation: random segregation (RSS) and trait-driven segregation (TSS). Extensions to diploid taxa, as well as various fitness landscapes and additional speciation modes will open a vast realm of potential applications. For instance, such a simulator can help answer longstanding questions about the impact and fate of microevolutionary processes on a macroevolutionary scale (Hansen and Martins, 1996; Arnold et al., 2001; Reznick and Ricklefs, 2009; Kostikova et al., 2016; Rolland et al., 2018; Duchen et al., 2018). Currently, our community lacks an individual-based simulator of phenotypic traits, although some research in this direction has been done in the past (Neuenschwander et al., 2008; Boucher et al., 2014). For instance, Neuenschwander et al. (2008) have developed a simulator of quantitative traits but they focus more on the genetic basis and works only at the population level. Additionally, Boucher et al. (2014) have also developed a simulator of phenotypes allowing for different modes of speciation, but limited to a

17

343 small number of generations. In this sense, our simulator is unique in that it

344 simulates populations of individuals for thousands of generations, and it allows for

345 speciation events to happen, thus generating complete phylogenies.

346 **Asymmetrical trait inheritance** Traditional macroevolutionary models

347 (including BM and OU), when run along phylogenetic trees, assume that the last

348 phenotypic value of a lineage and the starting values of its two daughter lineages are

349 identical (Felsenstein, 1973). However, we showed that when we consider species as

350 set of individuals each bearing its own phenotype, the resulting trait inheritance at

351 speciation will no longer be identical, and there are plenty of examples in nature

352 where this is the case (Galis and Metz, 1998; Lachaise et al., 1988; Schilthuizen, 2003;

353 Coyne and Orr, 2004; Ayoub et al., 2005; Jiggins et al., 2008; Givnish et al., 2009;

354 Serrano-Serrano et al., 2015). Consequently, when the segregation of individuals

355 between daughter species is random with respect to the trait value (our RSS

356 scenario), the expected amount of phenotypic change is small, although greater than

357 zero (Fig. 3). Yet, our simulations showed that even these small deviations from the

358 assumption of identical inheritance generate a substantial bias in the parameter

359 estimates under standard evolutionary models and alter the robustness of model

360 selection (Figs. 4, 5). While asymmetric inheritance has been theorized and modeled

361 explicitly for discrete traits (Goldberg and Igić, 2012), and biogeographic ranges (Ree

362 et al., 2005; Ree and Smith, 2008; Goldberg et al., 2011), this has not been formally

363 explored for quantitative traits.

364 **Effects of RSS** RSS generates jumps at lineage splits due to sampling effects

365 (Fig. 3). We found that even very small deviations from the parent phenotype can

366 alter the results of model fit (Fig. 4) and generate biased parameter estimations (Fig.

367 5). Traits simulated under a flat landscape and RSS generated less than 70% of

368 simulations fitting BM (Fig. 4, flat RSS). This scenario is supposed to fulfill all the

18

369   requirements for BM (equal fitness, no boundaries, and almost symmetrical

370   inheritance from parent to daughter species; Felsenstein, 1988; Boucher and Démery,

371   2016). However, we show here how the effect of random sampling of individuals

372   generates small variation in the mean phenotypes, and is enough to violate model

373   assumptions leading to the rejection of BM in a third of the simulations. The

374   RSS-normal scenario is consistent with the expectations of an OU model (normal

375   fitness landscape and almost symmetrical inheritance from parent to daughter

376   species; Hansen, 1997, but see Cooper et al. 2016) and indeed OU was the model of

377   choice in most cases.

378   **Effects of TSS**   Bigger deviations from the parent mean (as expected for TSS but

379   also for allopatric and peripatric speciations across phenotypic gradients; Fig 1B-D)

380   have more severe effects on both model selection and parameter estimation (Figs. 4

381   and 5, TSS cases). For instance, we found no support for the BM model under a flat

382   landscape, whereas models including the possibility of cladogenetic jumps were

383   favored, namely the κ model and, to a lesser extent, the Lévy model. Further, under

384   the TSS mode of speciation with normal landscape, the phenotypic jumps at

385   speciation appeared to disrupt the phylogenetic signal in most data sets with model

386   selection providing support for the WN model, i.e. a model in which phylogenetic

387   relationships do not contribute to explaining the trait values across species (Pennell

388   et al., 2014; Silvestro et al., 2015). This is clearly a failure of macroevolutionary

389   models to capture the true underlying process of evolution, which, in our simulations,

390   is instead entirely linked to parent-offspring inheritance and not based on a WN

391   underlying process.

392   **Modeling cladogenetic jumps**   While explicit models of cladogenetic and

393   anagenetic evolution exist (Bokma, 2008), their implementation is currently

394   unavailable. However, the κ transformation can capture cladogenetic change equally

395   well as long as phylogenies are complete (Harmon, 2018), which is the case in our

396   simulations. The limitation of the κ model is that it does not explicitly model the

397   jumps as a process (and, as a consequence, does not estimate a corrected rate of

398   anagenetic evolution σ^2, which is something Bokma's model should be able to do).

399   The Lévy process could fix part of the issue (Fig. 5B), but is unable to fully detect

400   jumps at all nodes, because it is designed to pick up rarer events of evolutionary

401   jumps (Duchen et al., 2017) instead of the more frequent events of cladogenetic jumps

402   simulated here. Additionally, under the normal landscape, there are no

403   implementations of models allowing us to jointly infer OU with jumps (an

404   implementation of the model of Bartoszek, 2014, would prove ideal in this case). As a

405   result, the best fitting model is often found to be a non-phylogenetic one (WN),

406   indicating that current comparative methods fail to detect phylogenetic signal, which

407   is blurred by jumps at speciation. Finally, both κ and Lévy do not exactly model the

408   process that we simulated, but are preferred because of an artifact, which is the

409   cladogenetic jumps generated by the natural sub-sampling of populations during a

410   lineage split. In other words, where BM and OU models should be the best fit,

411   TSS-induced jumps are blurring this signal. The same occurs under RSS if by chance

412   the jumps are large enough to bias the process. There is thus a clear need for the

413   development of new models that could account for such evolutionary processes.

414   **Punctuated equilibrium**   Jumps at speciation events are predicted by

415   "punctuated equilibrium", a theory that postulates that most of the phenotypic

416   change happens during cladogenesis (Gould and Eldredge, 1972, 1993). Since then, a

417   major debate argued whether phenotypic change was predominantly anagenetic or

418   cladogenetic (Uyeda et al., 2011), and new phylogenetic models to test these two

419   hypotheses were, thus, developed (Pagel, 1999; Bokma, 2008; Futuyma, 2010;

420   Bartoszek, 2014). This debate relies on adaptive jumps, while we were here concerned

421   with jumps generated by sub-sampling of individuals at speciation events, which

20

⁴²² could be both adaptive or neutral. Consequently, while the Lévy jump model could

⁴²³ detect evolutionary jumps at cladogenesis, it was not specifically designed to assess

⁴²⁴ jumps at speciation events as it models the occurrence of a jump as an anagenetic

⁴²⁵ process (Duchen et al., 2017; Landis and Schraiber, 2017). Additionally, the

⁴²⁶ sub-sampling effect of populations on macroevolution is not restricted to speciation

⁴²⁷ events only. Big changes in population sizes within branches of a phylogeny can also

⁴²⁸ generate jumps or "bursts" in phenotypic traits (Uyeda et al., 2011), thus making

⁴²⁹ this a more general issue.

The next generation of evolutionary models for quantitative traits

⁴³¹ While anagenetic evolutionary changes at the macroevolutionary level can be

⁴³² predicted by individual-based microevolutionary models (Rolland et al., 2018), it

⁴³³ remains unclear how microevolutionary models would justify identical inheritance at

⁴³⁴ speciation. These difficulties call for new models of macroevolution that account for

⁴³⁵ cladogenetic change and flexibility concerning the directionality of phenotypic

⁴³⁶ trajectories, i.e. flexibility concerning the fitness landscape of individuals in each

⁴³⁷ species (similar to the model of Boucher et al. 2017, but allowing for asymmetric trait

⁴³⁸ inheritance). Evolutionary models for discrete traits already account for non-identical

⁴³⁹ inheritance at speciation, such as the "Dispersal-Extinction-Cladogenesis" (DEC)

⁴⁴⁰ model (Ree et al., 2005; Ree and Smith, 2008), and the "Cladogenetic Stage change

⁴⁴¹ Speciation and Extinction" (ClaSSE) model (Goldberg and Igić, 2012). A continuous

⁴⁴² version of such models, that also include intra and interspecific variance (Kostikova

⁴⁴³ et al., 2016), would allow us to infer the link between micro and macroevolutionary

⁴⁴⁴ processes, which we formalized in the simulation framework presented here.

⁴⁴⁵ **Conclusion** We showed how different mechanisms of segregation of individuals

⁴⁴⁶ into species at a microevolutionary time scale, affect overall macroevolutionary

⁴⁴⁷ patterns across the entire phylogeny. The two modes of speciation we described here

21

likely represent two extremes of a spectrum, and we expect that the true processes of inheritance of phenotypic traits will lie somewhere within that range. However, we argue that ecologically relevant or geographically differentiated traits will be generally subject to some level of segregation at speciation. Our results highlight the sensitivity of comparative methods to small variations in the inheritance of trait values between parent and daughter species, and call for caution when interpreting model testing and parameter estimation in macroevolution. In the light of the effects of differential trait segregation at speciation shown here, we propose the next generation of comparative methods incorporate asymmetric inheritance as a fundamental component of the evolutionary process.

Acknowledgements

Code and data availability

All the data and codes associated with this paper including meta-data and a tutorial to run the simulations are available at:

https://bitbucket.org/daniele_silvestro/phylotraitsimulator/src/master/

References

Arnold, S. J., M. E. Pfrender, and A. G. Jones. 2001. The adaptive landscape as a conceptual bridge between micro-and macroevolution. Pages 9–32 *in* Microevolution rate, pattern, process. Springer.

Ayoub, N. A., S. E. Riechert, and R. L. Small. 2005. Speciation history of the North American funnel web spiders, Agelenopsis (Araneae: Agelenidae): Phylogenetic inferences at the population–species interface. Molecular Phylogenetics and Evolution 36:42–57.

Bartoszek, K. 2014. Quantifying the effects of anagenetic and cladogenetic evolution. Mathematical biosciences 254:42–57.

Beaulieu, J. M., D.-C. Jhwueng, C. Boettiger, and B. C. O'Meara. 2012. Modeling stabilizing selection: expanding the ornstein–uhlenbeck model of adaptive evolution. Evolution: International Journal of Organic Evolution 66:2369–2383.

Bokma, F. 2008. Detection of "punctuated equilibrium" by bayesian estimation of speciation and extinction rates, ancestral character states, and rates of anagenetic and cladogenetic evolution on a molecular phylogeny. Evolution: International Journal of Organic Evolution 62:2718–2726.

Boucher, F. C. and V. Démery. 2016. Inferring bounded evolution in phenotypic characters from phylogenetic comparative data. Systematic biology 65:651–661.

Boucher, F. C., V. Démery, E. Conti, L. J. Harmon, and J. Uyeda. 2017. A general model for estimating macroevolutionary landscapes. Systematic biology 67:304–319.

Boucher, F. C., W. Thuiller, T. J. Davies, and S. Lavergne. 2014. Neutral biogeography and the evolution of climatic niches. The American Naturalist 183:573–584.

23

Campbell, S. A. and A. Kessler. 2013. Plant mating system transitions drive the macroevolution of defense strategies. Proceedings of the National Academy of Sciences Page 201213867.

Cooper, N., G. H. Thomas, C. Venditti, A. Meade, and R. P. Freckleton. 2016. A cautionary note on the use of Ornstein Uhlenbeck models in macroevolutionary studies. Biological Journal of the Linnean Society 118:64–77.

Coyne, J. and H. Orr. 2004. Speciation. Sinauer Associates Sunderland, MA.

Duchen, P., S. Hautphenne, L. Lehmann, and N. Salamin. 2018. Linking micro and macroevolution in the presence of migration. bioRxiv Page 490128.

Duchen, P., C. Leuenberger, S. M. Szilágyi, L. Harmon, J. Eastman, M. Schweizer, and D. Wegmann. 2017. Inference of evolutionary jumps in large phylogenies using Lévy processes. Systematic Biology 66:950–963.

Eastman, J. M., M. E. Alfaro, P. Joyce, A. L. Hipp, and L. J. Harmon. 2011. A novel comparative method for identifying shifts in the rate of character evolution on trees. Evolution: International Journal of Organic Evolution 65:3578–3589.

Etienne, R. S., B. Haegeman, T. Stadler, T. Aze, P. N. Pearson, A. Purvis, and A. B. Phillimore. 2011. Diversity-dependence brings molecular phylogenies closer to agreement with the fossil record. Proceedings of the Royal Society B: Biological Sciences 279:1300–1309.

Felsenstein, J. 1973. Maximum-likelihood estimation of evolutionary trees from continuous characters. American Journal of Human Genetics 25:471.

Felsenstein, J. 1985. Phylogenies and the comparative method. The American Naturalist 125:1–15.

516 Felsenstein, J. 1988. Phylogenies and quantitative characters. Annual Review of
517   Ecology and Systematics 19:445–471.

518 Felsenstein, J. 2004. Inferring phylogenies vol. 2. Sinauer associates Sunderland, MA.

519 Futuyma, D. J. 2010. Evolutionary constraint and ecological consequences. Evolution:
520   International Journal of Organic Evolution 64:1865–1884.

521 Futuyma, D. J. and A. A. Agrawal. 2009. Macroevolution and the biological diversity
522   of plants and herbivores. Proceedings of the National Academy of Sciences
523   Pages pnas–0904106106.

524 Galis, F. and J. A. Metz. 1998. Why are there so many cichlid species? Trends in
525   Ecology & Evolution 13:1–2.

526 Garland, T., A. W. Dickerman, C. M. Janis, and J. A. Jones. 1993. Phylogenetic
527   analysis of covariance by computer simulation. Systematic Biology 42:265–292.

528 Givnish, T. J., K. C. Millam, A. R. Mast, T. B. Paterson, T. J. Theim, A. L. Hipp,
529   J. M. Henss, J. F. Smith, K. R. Wood, and K. J. Sytsma. 2009. Origin, adaptive
530   radiation and diversification of the hawaiian lobeliads (asterales: Campanulaceae).
531   Proceedings of the Royal Society B: Biological Sciences 276:407–416.

532 Goldberg, E. E. and B. Igić. 2012. Tempo and mode in plant breeding system
533   evolution. Evolution: International Journal of Organic Evolution 66:3701–3709.

534 Goldberg, E. E., L. T. Lancaster, and R. H. Ree. 2011. Phylogenetic inference of
535   reciprocal effects between geographic range evolution and diversification.
536   Systematic Biology 60:451–465.

537 Gould, S. J. and N. Eldredge. 1972. Punctuated equilibria: an alternative to phyletic
538   gradualism. Essential readings in evolutionary biology Pages 82–115.

25

539 Gould, S. J. and N. Eldredge. 1993. Punctuated equilibrium comes of age. Nature
540   366:223.

541 Hansen, T. F. 1997. Stabilizing selection and the comparative analysis of adaptation.
542   Evolution 51:1341–1351.

543 Hansen, T. F. and E. P. Martins. 1996. Translating between microevolutionary
544   process and macroevolutionary patterns: the correlation structure of interspecific
545   data. Evolution 50:1404–1417.

546 Harmon, L. 2018. Phylogenetic comparative methods: learning from trees.
547   EcoEvoRxiv.

548 Harmon, L. J., J. B. Losos, T. Jonathan Davies, R. G. Gillespie, J. L. Gittleman,
549   W. Bryan Jennings, K. H. Kozak, M. A. McPeek, F. Moreno-Roark, T. J. Near,
550   et al. 2010. Early bursts of body size and shape evolution are rare in comparative
551   data. Evolution: International Journal of Organic Evolution 64:2385–2396.

552 Harvey, P. H., M. D. Pagel, et al. 1991. The comparative method in evolutionary
553   biology vol. 239. Oxford university press Oxford.

554 Jiggins, C. D., C. Salazar, M. Linares, and J. Mavarez. 2008. Hybrid trait speciation
555   and heliconius butterflies. Philosophical Transactions of the Royal Society B:
556   Biological Sciences 363:3047–3054.

557 Katzourakis, A., R. J. Gifford, M. Tristem, M. T. P. Gilbert, and O. G. Pybus. 2009.
558   Macroevolution of complex retroviruses. Science 325:1512–1512.

559 Kingsley, M., J. Nagy, and R. Russell. 1983. Patterns of weight gain and loss for
560   grizzly bears in northern Canada. Bears: Their Biology and Management
561   Pages 174–178.

26

Kostikova, A., D. Silvestro, P. B. Pearman, and N. Salamin. 2016. Bridging inter-and intraspecific trait evolution with a hierarchical bayesian approach. Systematic biology 65:417–431.

Lachaise, D., M.-L. Cariou, J. R. David, F. Lemeunier, L. Tsacas, and M. Ashburner. 1988. Historical biogeography of the *Drosophila melanogaster* species subgroup. Pages 159–225 *in* Evolutionary biology. Springer.

Lande, R. 1976. Natural selection and random genetic drift in phenotypic evolution. Evolution 30:314–334.

Lande, R. 1980. Microevolution in relation to macroevolution. Paleobiology 6:233–238.

Landis, M. J. and J. G. Schraiber. 2017. Pulsed evolution shaped modern vertebrate body sizes. Proceedings of the National Academy of Sciences 114:13224–13229.

Landis, M. J., J. G. Schraiber, and M. Liang. 2012. Phylogenetic analysis using Lévy processes: finding jumps in the evolution of continuous traits. Systematic biology 62:193–204.

Losos, J. B. 2011. Lizards in an evolutionary tree: ecology and adaptive radiation of anoles vol. 10. Univ of California Press.

McCarthy, T. M., L. P. Waits, and B. Mijiddorj. 2009. Status of the Gobi bear in Mongolia as determined by noninvasive genetic methods. Ursus 20:30–39.

Neuenschwander, S., F. Hospital, F. Guillaume, and J. Goudet. 2008. quantinemo: an individual-based program to simulate quantitative traits with explicit genetic architecture in a dynamic metapopulation. Bioinformatics 24:1552–1553.

O'Meara, B. C. 2012. Evolutionary inferences from phylogenies: a review of methods. Annual Review of Ecology, Evolution, and Systematics 43:267–285.

27

O'Meara, B. C., C. Ané, M. J. Sanderson, and P. C. Wainwright. 2006. Testing for different rates of continuous trait evolution using likelihood. Evolution 60:922–933.

O'Meara, B. C. and J. M. Beaulieu. 2014. Modelling stabilizing selection: the attraction of ornstein–uhlenbeck models. Pages 381–393 *in* Modern phylogenetic comparative methods and their application in evolutionary biology. Springer.

Pagel, M. 1999. Inferring the historical patterns of biological evolution. Nature 401:877.

Pennell, M. W., J. M. Eastman, G. J. Slater, J. W. Brown, J. C. Uyeda, R. G. FitzJohn, M. E. Alfaro, and L. J. Harmon. 2014. geiger v2. 0: an expanded suite of methods for fitting macroevolutionary models to phylogenetic trees. Bioinformatics 30:2216–2218.

Ree, R. H., B. R. Moore, C. O. Webb, and M. J. Donoghue. 2005. A likelihood framework for inferring the evolution of geographic range on phylogenetic trees. Evolution 59:2299–2311.

Ree, R. H. and S. A. Smith. 2008. Maximum likelihood inference of geographic range evolution by dispersal, local extinction, and cladogenesis. Systematic biology 57:4–14.

Revell, L. J. 2012. phytools: an r package for phylogenetic comparative biology (and other things). Methods in Ecology and Evolution 3:217–223.

Reznick, D. N. and R. E. Ricklefs. 2009. Darwin's bridge between microevolution and macroevolution. Nature 457:837.

Rolland, J., D. Silvestro, G. Litsios, L. Faye, and N. Salamin. 2018. Clownfishes evolution below and above the species level. Proceedings of the Royal Society B: Biological Sciences 285:20171796.

28

610   Schilthuizen, M. 2003. Shape matters: the evolution of insect genitalia. Pages 9–16 *in*
611   Proceedings Of The Section Experimental And Applied Entomology-Netherlands
612   Entomological Society vol. 14.

613   Serrano-Serrano, M. L., M. Perret, M. Guignard, A. Chautems, D. Silvestro, and
614   N. Salamin. 2015. Decoupled evolution of floral traits and climatic preferences in a
615   clade of neotropical gesneriaceae. BMC evolutionary biology 15:247.

616   Serrano-Serrano, M. L., J. Rolland, J. L. Clark, N. Salamin, and M. Perret. 2017.
617   Hummingbird pollination and the diversification of angiosperms: an old and
618   successful association in gesneriaceae. Proceedings of the Royal Society B:
619   Biological Sciences 284:20162816.

620   Silvestro, D., A. Kostikova, G. Litsios, P. B. Pearman, and N. Salamin. 2015.
621   Measurement errors should always be incorporated in phylogenetic comparative
622   analysis. Methods in Ecology and Evolution 6:340–346.

623   Silvestro, D., M. F. Tejedor, M. L. Serrano-Serrano, O. Loiseau, V. Rossier,
624   J. Rolland, A. Zizka, S. Hoehna, A. Antonelli, and N. Salamin. 2018. Early arrival
625   and climatically-linked geographic expansion of New World monkeys from tiny
626   African ancestors. Syst Biol Page doi:10.1093/sysbio/syy046.

627   Simpson, G. G. 1944. Tempo and mode in evolution. 15 Columbia University Press.

628   Slater, G. J. 2013. Phylogenetic evidence for a shift in the mode of mammalian body
629   size evolution at the Cretaceous-Palaeogene boundary. Methods in Ecology and
630   Evolution 4:734–744.

631   Slater, G. J., L. J. Harmon, D. Wegmann, P. Joyce, L. J. Revell, and M. E. Alfaro.
632   2012. Fitting models of continuous trait evolution to incompletely sampled
633   comparative data using approximate Bayesian computation. Evolution:
634   International Journal of Organic Evolution 66:752–762.

635   Stanley, S. M. 1979. Macroevolution, pattern and process. Johns Hopkins University
636   Press.

637   Svensson, E. and R. Calsbeek. 2012. The adaptive landscape in evolutionary biology.
638   Oxford University Press.

639   Uyeda, J. C., T. F. Hansen, S. J. Arnold, and J. Pienaar. 2011. The million-year wait
640   for macroevolutionary bursts. Proceedings of the National Academy of Sciences
641   Page 201014503.

642   Venditti, C., A. Meade, and M. Pagel. 2011. Multiple routes to mammalian diversity.
643   Nature 479:393.

644   Wagner, P. J. 2017. Vertebrate body size jumps the Wright way. Proceedings of the
645   National Academy of Sciences 114:13068–13070.

646   Wasserthal, L. 1997. The pollinators of the Malagasy star orchids *Angraecum*
647   *sesquipedale*, *A. sororium* and *A. compactum* and the evolution of extremely long
648   spurs by pollinator shift. Botanica Acta 110:343–359.

Supplementary Information
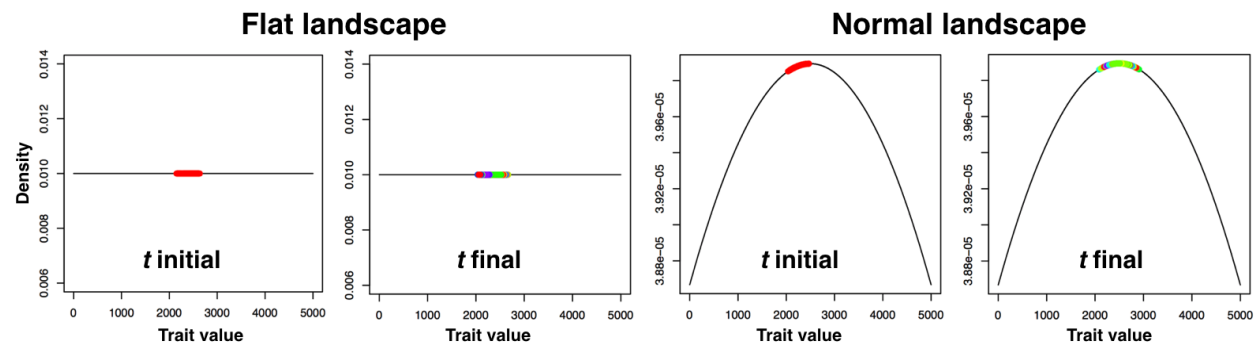
A Supplementary figures

Figure 6: Fitness landscapes. Left: Flat landscape with the initial population (red points) and the set of species at the end of the simulation run (maintaining the same initial mean trait). Right: Normal landscape, where the final set of species has moved to the top of the landscape when compared to the initial values.
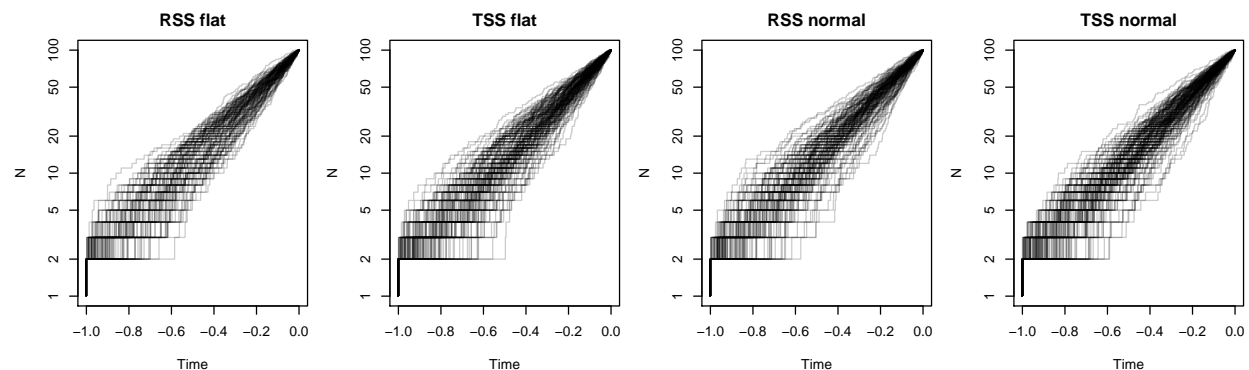

Figure 7: Lineage-through-time (LTT) plots of all simulations under all four scenarios: RSS flat, TSS flat, RSS normal, and TSS normal.
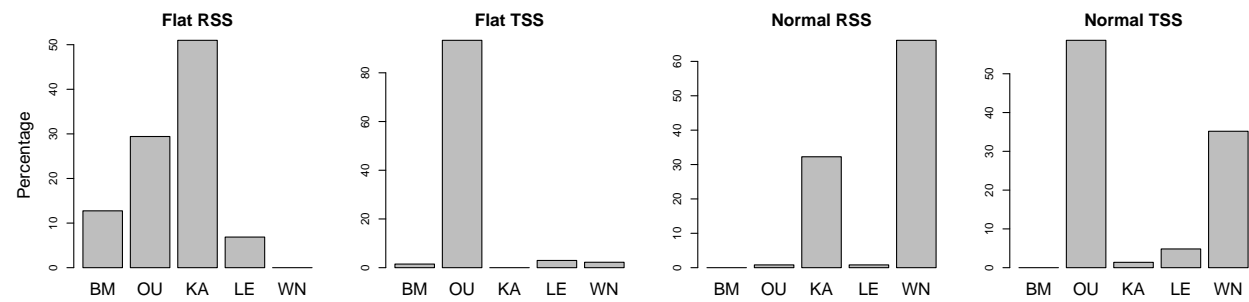
31

Figure 8: Second best fit under all four scenarios. Bars represent the percentage of simulations that were second best fit by a given model. Abbreviations: BM = Brownian Motion, OU = Ornstein-Uhlenbeck, KA = Kappa, LE = Lévy, and WN = White Noise.
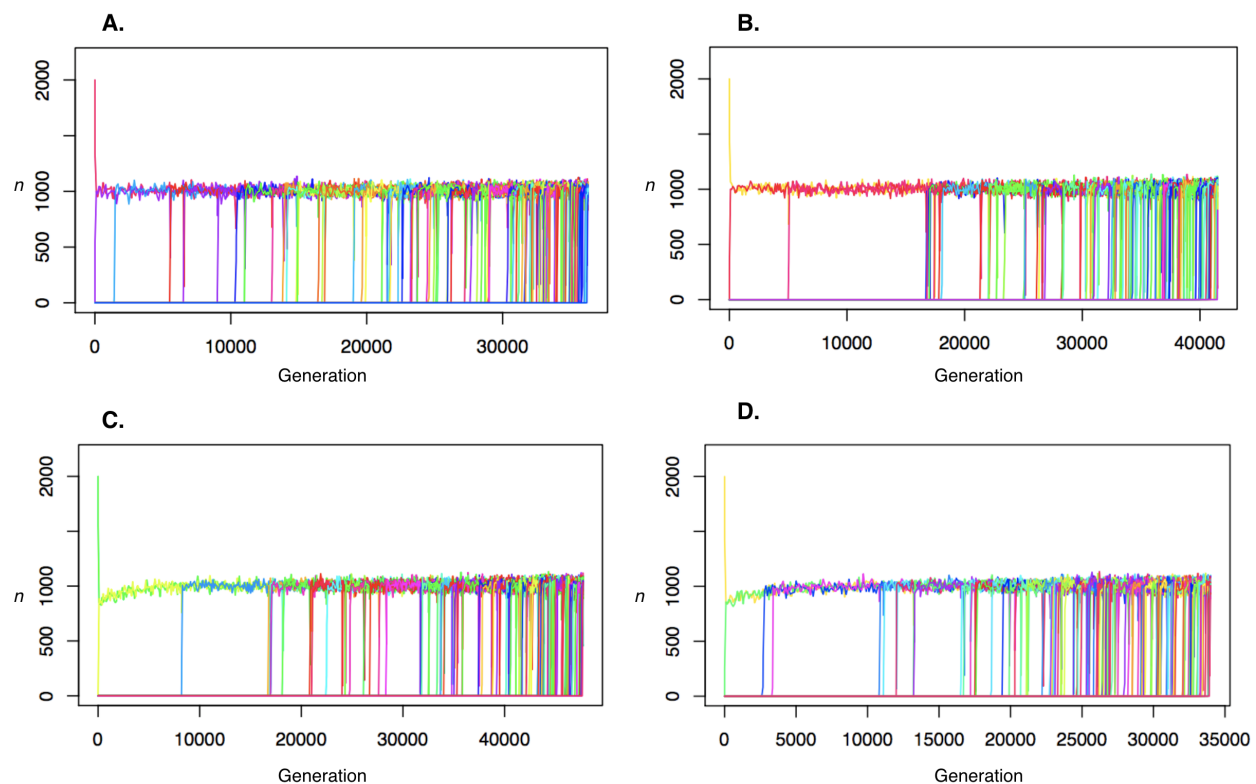

Figure 9: Change in population sizes n over time. A. RSS flat, B. TSS flat, C. RSS normal, D. TSS normal. Note how the carrying capacity $K = 1000$ is reached very quickly.